Electronic phase transitions and magnetoresistance in a new bilayer manganate, $Ca_{2.5}Sr_{0.5}GaMn_2O_8$

2002 J. Phys.: Condens. Matter 14 13569

(http://iopscience.iop.org/0953-8984/14/49/312)

INSTITUTE OF PHYSICS PUBLISHING JOURNAL OF PHYSICS: CONDENSED MATTER

J. Phys.: Condens. Matter **14** (2002) 13569–13577 PII: S0953-8984(02)53906-0

Electronic phase transitions and magnetoresistance in a new bilayer manganate, $Ca_{2.5}Sr_{0.5}GaMn_2O_8$

Peter D Battle[1], Stephen J Blundell[2], P N Santhosh[1], Matthew J Rosseinsky[3] and Christopher Steer[2]

[1] Inorganic Chemistry Laboratory, Department of Chemistry, Oxford University, South Parks Road, Oxford OX1 3QR, UK
[2] Clarendon Laboratory, Department of Physics, Oxford University, Parks Road, Oxford OX1 3PU, UK
[3] Department of Chemistry, University of Liverpool, Liverpool L69 7ZD, UK

Received 25 September 2002
Published 29 November 2002
Online at stacks.iop.org/JPhysCM/14/13569

Abstract

The crystal structure of the anion-deficient perovskite $Ca_{2.5}Sr_{0.5}GaMn_2O_8$ has been studied at 290 and 5 K by neutron diffraction (290 K; space group $Pcm2_1$, $a = 5.4294(1)$, $b = 11.3722(3)$, $c = 5.2983(1)$ Å). The vacant oxide sites order to create a structure in which perovskite bilayers consisting of MnO_6 octahedra are isolated from each other along [010] by a single layer of GaO_4 tetrahedra. At 5 K the material is antiferromagnetic with an ordered magnetic moment of 3.09(1) μ_B per Mn cation. Magnetic susceptibility measurements suggest that short-range magnetic ordering within the bilayers occurs above 200 K, and muon spin relaxation data show that the transition to long-range magnetic order occurs between 150 and 125 K. The resistivity of $Ca_{2.5}Sr_{0.5}GaMn_2O_8$ decreases by an order of magnitude at 125 K, and ∼50% magnetoresistance is seen in a field of 80 kOe at 110 K.

(Some figures in this article are in colour only in the electronic version)

A material whose electrical resistivity is a function of the applied magnetic field can have applications in spin valves, field sensing and data storage. In recent years, the search for new magnetoresistive materials has expanded to include mixed-metal oxides, particularly mixed-valence oxides of manganese. This research has largely focused on two members of the $A_{n+1}Mn_nO_{3n+1}$ Ruddlesden–Popper (RP) series, namely the $n = \infty$ perovskites, for example $(La_{1-x}Sr_x)MnO_3$ [1] and the $n = 2$ phases, for example $(Sr_{1.8}La_{1.2})Mn_2O_7$ [2]. These compounds show what has become known as colossal magnetoresistance (CMR), that is $(\rho(0)-\rho(H))/\rho(0) \sim 90\%$. The perovskites [3] exhibit this behaviour at room temperature, but only in fields of ∼100 kOe, whereas the $n = 2$ phases [4] are active in magnetic fields of less than 10 kOe, but only at temperatures below 150 K. The challenge is clearly to produce a material which can operate in low fields at room temperature. In order to do this we have

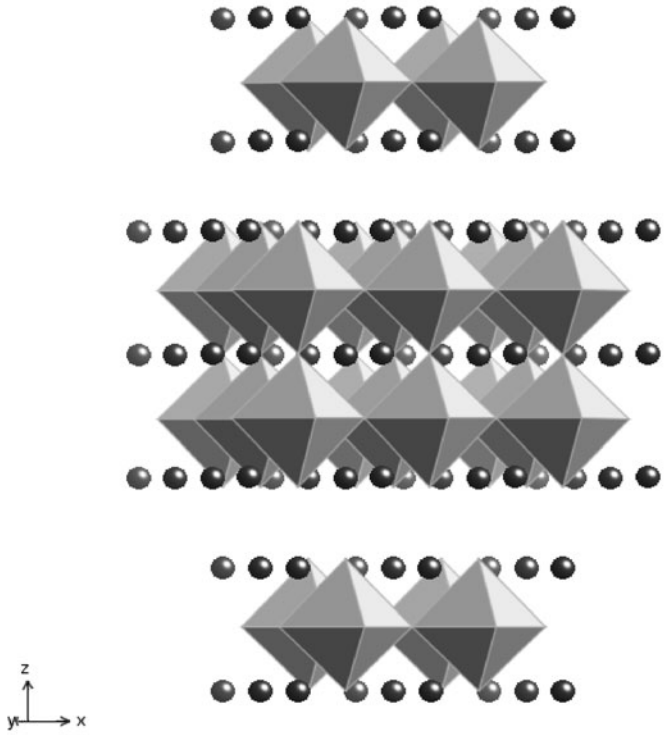

Figure 1. Crystal structure of the $n = 2$ RP phase $A_3Mn_2O_7$ showing perovskite bilayers separated by AO layers; MnO_6 octahedra are lightly shaded, filled circles represent A cations.

adopted a strategy of searching for mixed-valence compounds in which key structural features of both the perovskites and the $n = 2$ manganates are retained. The crystal structure of the latter is comprised (figure 1) of perovskite-like blocks, each consisting of 2 (i.e. n) layers of vertex-sharing MnO_6 octahedra, with neighbouring blocks being isolated from each other along the [001] axis of the tetragonal unit cell by electronically inactive, diamagnetic, ionic layers of composition (Sr, La)O. The work described below was motivated by a knowledge of the crystal structure of $(Ca_2La)Fe_3O_8$ [5], which is an anion-deficient perovskite with an ordered arrangement of oxide vacancies; the Ca and La cations occupy the A sites in a disordered manner. The ordering of anion vacancies results in an orthorhombic structure in which double layers of FeO_6 octahedra are separated by layers of FeO_4 tetrahedra; that is, the vacancies occur in every third layer, aligned in rows along a $\langle 110 \rangle$ direction of the simple cubic perovskite unit cell. We report below the synthesis and characterization of isostructural $(Ca_{2.5}Sr_{0.5})GaMn_2O_8$. In this compound the diamagnetic d^{10} cation Ga^{3+} has replaced Fe^{3+} on the tetrahedral sites and the reduction in total charge on the A sites has facilitated the introduction of a 1:1 mixture of Mn^{3+} and Mn^{4+} on the octahedral sites. We have thus achieved our aim of accommodating isolated, mixed-valence Mn bilayers in a perovskite-related crystal structure without introducing ionic separating layers. The resistivity of the new material falls by an order of magnitude on cooling below 125 K, a temperature which is close to the Néel point, and a magnetoresistance of $\sim$50% is observed in 80 kOe at 108 K. The observation of these properties in an arbitrarily chosen composition suggests that chemical tuning of the stoichiometry might produce related materials with significant electronic properties.

Table 1. Atomic coordinates of $Ca_{2.5}Sr_{0.5}GaMn_2O_8$ at 290 K. Space group $Pcm2_1$, $a = 5.4294(1)$, $b = 11.3722(3)$, $c = 5.2983(1)$ Å; $R_{wp} = 5.25\%$, $\chi^2 = 3.04$.

Atom	x	y	z	$100 \times U_{iso}$ (Å^2)
Ca	0.2226(6)	0.1863(2)	0.508(2)	0.33(6)
Ca/Sr[a]	0.2394(7)	0.5	0.491(2)	0.36(6)
Mn	0.2579(9)	0.3298(3)	0	0.61(8)
Ga	0.3204(6)	0	0.051(2)	0.9(1)
O1	0.3654(8)	0	0.403(2)	1.1(1)
O2	0.3025(8)	0.5	−0.005(2)	1.0(1)
O3	0.1867(5)	0.1431(2)	−0.025(2)	0.91(6)
O4	−0.0030(7)	0.3432(2)	0.243(2)	0.51(6)
O5	0.4940(8)	0.3072(2)	0.249(2)	0.70(6)

[a] Random distribution in a 1:1 ratio.

$Ca_{2.5}Sr_{0.5}GaMn_2O_8$ was prepared by firing stoichiometric quantities of $CaCO_3$, $SrCO_3$, MnO_2 and Ga_2O_3 in alumina crucibles, initially at 1000 °C and subsequently in pellet form for 192 h at 1100 °C in air. X-ray powder diffraction data were collected on a Philips PW1710 diffractometer, operating with Cu Kα radiation in Bragg–Brentano geometry. Neutron powder diffraction data were collected at a wavelength of 1.5938 Å using the diffractometer D2b at ILL Grenoble. All the diffraction data were analysed using the Rietveld [6] method, as implemented in the GSAS [7] program suite. Magnetic measurements were performed on a Quantum Design MPMS 5000 SQUID magnetometer between 0 and 50 kOe and 5 and 350 K. Resistivity and magnetotransport measurements were carried out on a sintered bar using the four-wire method. The sample was mounted in a variable temperature insert which was located in a 16 T superconducting magnet. The applied ac (<10 μA) was perpendicular to the applied magnetic field. Muon spin relaxation (μSR) data were taken on the Argus pulsed muon beamline at the ISIS facility at the Rutherford Appleton Laboratory. A beam of completely polarized muons was implanted with momentum 28 MeV/c into the sample under investigation. The muons stop suddenly ($<10^{-9}$ s) without loss of spin polarization. The muon then decays, with a half-life of 2.2 μs, and emits a positron, preferentially in the direction of the muon spin at the moment of decay. By measuring the number of counts (positrons) in a bank of forward and backward detectors the emitted positron asymmetry is studied [8]. The observed quantity is the time-dependent asymmetry, $A_R(t)$, which is proportional to the autocorrelation function of the muon spin polarization. The dynamics of the internal field are probed because the muon precesses around the instantaneous field direction. The magnetic field of the Earth is compensated for to an accuracy of 10 μT.

We originally attempted to prepare the composition $Ca_3GaMn_2O_8$ in a high-temperature solid state reaction. Initial characterization by x-ray powder diffraction indicated that the reaction product was monophasic, but subsequent magnetic susceptibility measurements revealed the presence of small quantities ($\sim$5%) of $CaMnO_{3-\delta}$, which develops [9] a readily detected spontaneous magnetization on cooling below 125 K. Closer scrutiny of the x-ray data confirmed the presence of this minority phase. In an effort to eliminate the impurity we prepared $Ca_{3-x}Sr_xGaMn_2O_8$ ($0 \leqslant x \leqslant 0.6$) and established, on the basis of magnetization data, that the $CaMnO_{3-\delta}$ content is minimized ($\sim$1%) in $Ca_{2.5}Sr_{0.5}GaMn_2O_8$. All further measurements were carried out on samples having this composition and impurity level. The room temperature crystal structure (tables 1 and 2, and figure 2) was refined from neutron powder diffraction data; the $CaMnO_{3-\delta}$ concentration lies close to the detection limit of this technique and the impurity was not detectable in these data. $Sr_2LaFe_3O_8$ was previously [10] modelled in a centrosymmetric space group, albeit with a disordered anion sublattice, but

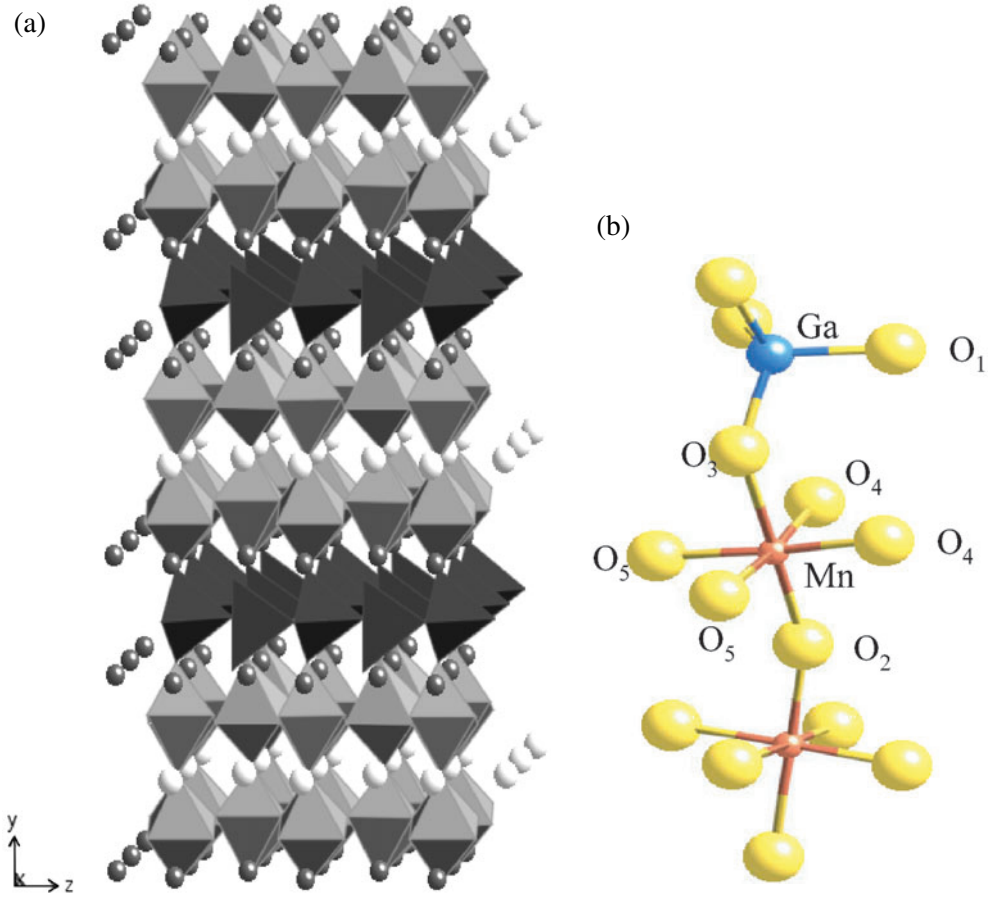

Figure 2. Room temperature crystal structure of $Ca_{2.5}Sr_{0.5}GaMn_2O_8$. (a) Polyhedral representation with MnO_6 octahedra and GaO_4 tetrahedra shaded light and dark, respectively. Light circles represent Ca/Sr cations, dark circles Ca only. (b) Local coordination around the Mn and Ga sites.

the structure of $Ca_{2.5}Sr_{0.5}GaMn_2O_8$ was better modelled in the non-centrosymmetric space group $Pcm2_1$, with no disorder. The two cation species occupying the A sites order, with all the Sr being located within the perovskite bilayers. A-site ordering was observed in neither $Ca_2LaFe_3O_8$ nor $Sr_2LaFe_3O_8$ [5, 10], and is regarded as rare in perovskites; it is more common in $n = 2$ RP phases [11]. The range of Mn–O bond lengths in the MnO_6 octahedra can be parametrized using the distortion parameter

$$\sigma_{JT} = \sqrt{\tfrac{1}{6}\sum_i [(\text{Mn–O})_i - \langle \text{Mn–O} \rangle]^2}$$

which takes a value of 0.096. This is smaller than the value (0.186) observed in $SrCaMnGaO_5$, a related, single-layer orthorhombic compound with the Jahn–Teller cation Mn^{3+} occupying all the octahedral sites, rather than half of them as in $Ca_{2.5}Sr_{0.5}GaMn_2O_8$. More surprisingly, it is also smaller than the value (0.15) observed in $Sr_2LaFe_3O_8$, which does not contain any Jahn–Teller cations. The longest Mn–O bond (Mn–O3, 2.163 Å) is directed out of the bilayer, as is the case in the majority of $n = 2$ RP phases, while the two shortest bonds (Mn–O5) form

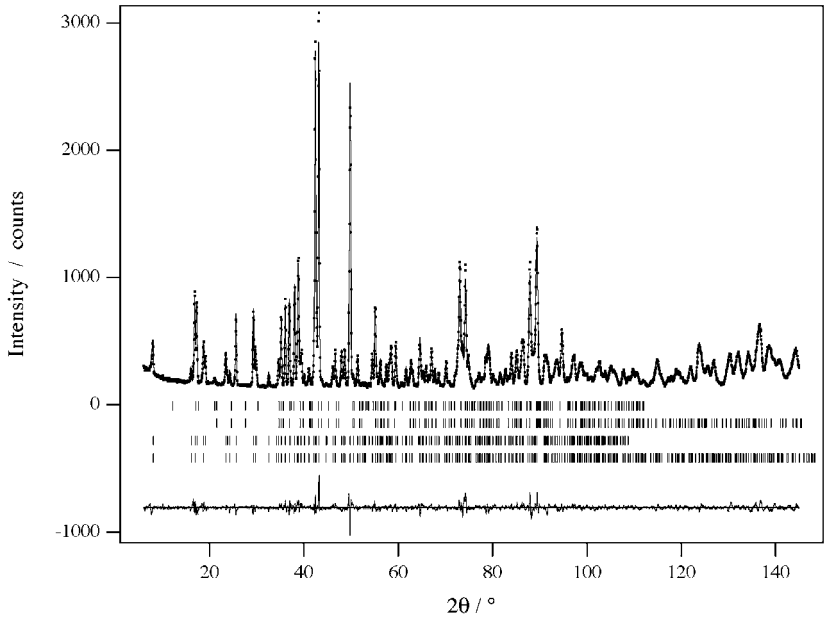

Figure 3. Observed (●), calculated (——) and difference neutron diffraction profiles of $Ca_{2.5}Sr_{0.5}GaMn_2O_8$ at 5 K. Reflection positions correspond to (top to bottom): $CaMnO_{3-\delta}$ magnetic, $CaMnO_{3-\delta}$ structural, $Ca_{2.5}Sr_{0.5}GaMn_2O_8$ magnetic, $Ca_{2.5}Sr_{0.5}GaMn_2O_8$ structural.

Table 2. Bond lengths and angles in $Ca_{2.5}Sr_{0.5}GaMn_2O_8$ at 290 K.

Mn–O (Å)		Ga–O (Å)		Bond angles (deg)	
Mn–O2	1.950(4)	Ga–O1	1.881(5)	Mn–O2–Mn	165.7(5)
Mn–O3	2.163(5)		1.877(5)	Mn–O4–Mn	170.7(3)
Mn–O4	1.920(10)			Mn–O5–Mn	165.2(3)
	1.948(10)	Ga–O3	1.827(3)		
Mn–O5	1.857(10)		1.827(3)	Ga–O1–Ga	122.2(3)
	1.910(10)			Mn–O3–Ga	142.2(3)

a *cis* pair within the layers. In addition to the wide variation in bond lengths observed in the MnO_6 octahedra, the orthorhombic symmetry leads to greater non-linearity in the Mn–O–Mn bond angles (which range between 165.2° and 170.7°) than is observed in $n = 2$ RP phases or $SrCaMnGaO_5$; these angles are likely to be significant in determining the nature of the magnetic ordering described below. A neutron diffraction pattern recorded at 5 K contained additional peaks at low angles. One of the weakest of these peaks was attributable to magnetic scattering from $CaMnO_{3-\delta}$, thus allowing the contribution from this phase to be allowed for in the data analysis. The other low angle peaks could be accounted for (figure 3) by assuming that the Mn magnetic moments in $Ca_{2.5}Sr_{0.5}GaMn_2O_8$ align along [010] in the antiferromagnetic spin structure shown in figure 4. Each Mn cation is coupled antiferromagnetically to the four nearest-neighbour cations in the same *xz* sheet, and ferromagnetically to the single nearest neighbour in the other sheet of the same bilayer; the inter-bilayer coupling through the GaO_4 tetrahedra is ferromagnetic. The mean ordered moment of the Mn cations refined to a value of 3.09(1) μ_B, which is consistent with the presence of a 1:1 ratio of Mn^{3+} and Mn^{4+}

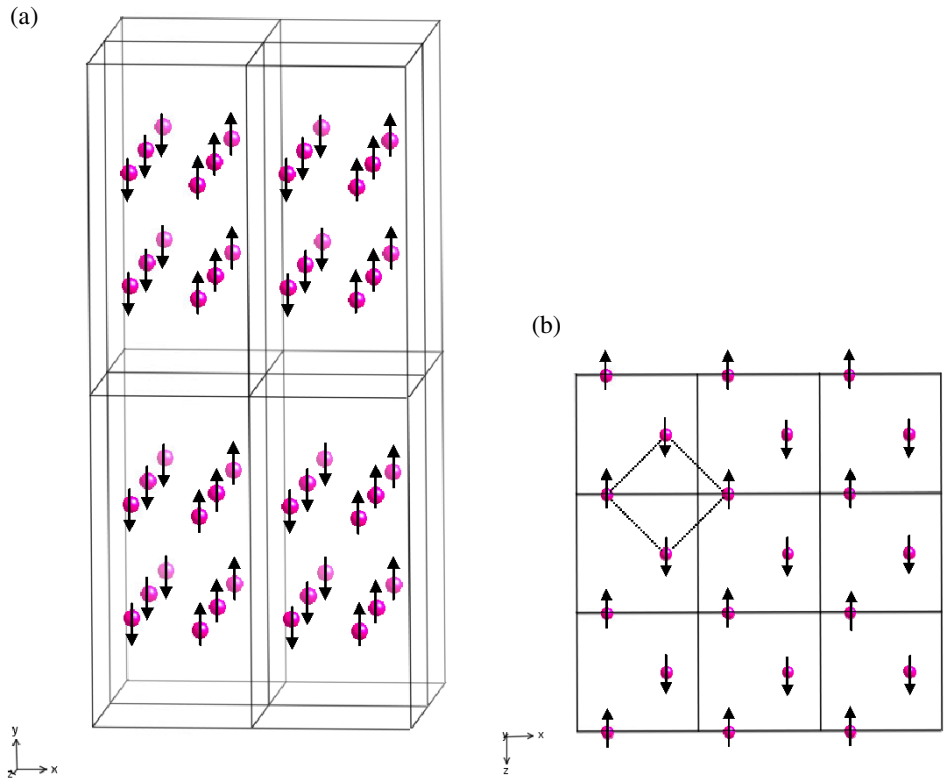

Figure 4. Magnetic structure of $Ca_{2.5}Sr_{0.5}GaMn_2O_8$ viewed (a) perpendicular to [010] and (b) along [010]. Only Mn cations are shown. Arrows in (b) represent only *relative* spin directions.

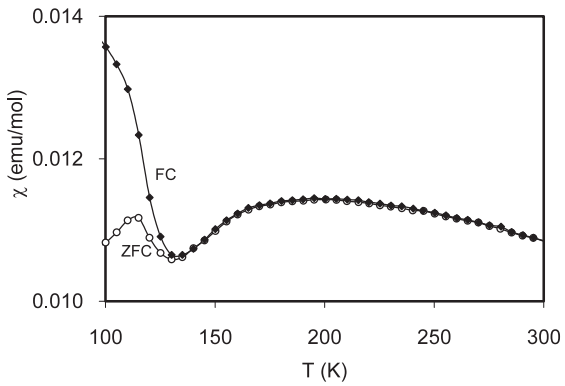

Figure 5. Temperature dependence of molar magnetic susceptibility of $Ca_{2.5}Sr_{0.5}GaMn_2O_8$ measured in 100 Oe after zero field cooling (ZFC) and field cooling (FC).

cations. The crystal structure did not change significantly ($a = 5.4165(2)$, $b = 11.3639(7)$, $c = 5.2841(2)$ Å; $R_{wp} = 5.26\%$, $\chi^2 = 3.907$) on cooling from 300 to 5 K; there was no evidence for long-range charge ordering, although it should be noted that the charge-ordered state in the $n = 2$ systems is only observed over a restricted temperature range because of competition with incompatible orbital ordering [12–14]. The magnetic susceptibility (figure 5)

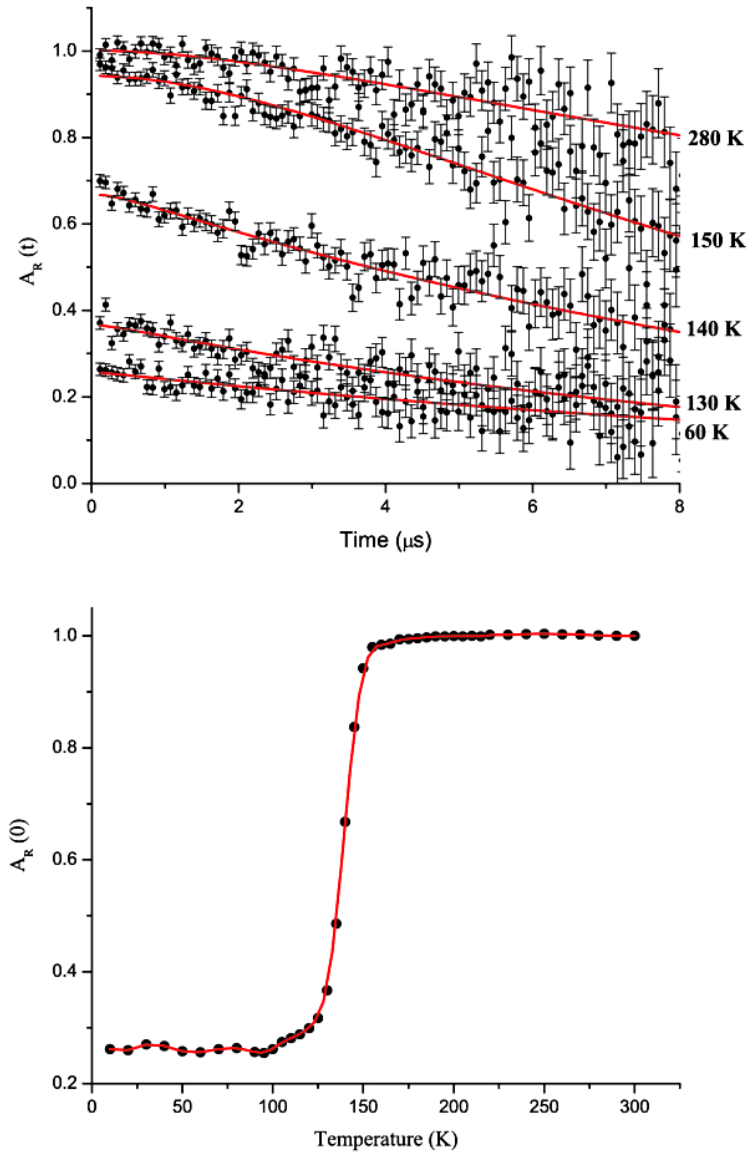

Figure 6. (a) Time dependence of the μSR relaxing asymmetry as a function of temperature. (b) Temperature dependence of the initial relaxing asymmetry.

of the sample clearly shows the magnetic phase transition of the impurity phase at 125 K [9]; the magnitude of the low-temperature magnetization is consistent with a 1% impurity level. We attribute the broad susceptibility maximum observed between 125 and 300 K to the onset of antiferromagnetic ordering in the principal phase. The width of the maximum suggests that short-range ordering occurs, perhaps within individual bilayers, before long-range 3D order is established. The temperature at which long-range ordering occurs is not clear from the susceptibility data. However, weak magnetic Bragg peaks (consistent with the 5 K magnetic structure of $Ca_{2.5}Sr_{0.5}GaMn_2O_8$) and low-angle diffuse scattering were apparent in neutron diffraction data collected at 150 K. Furthermore, μSR data (figure 6) show that the transition

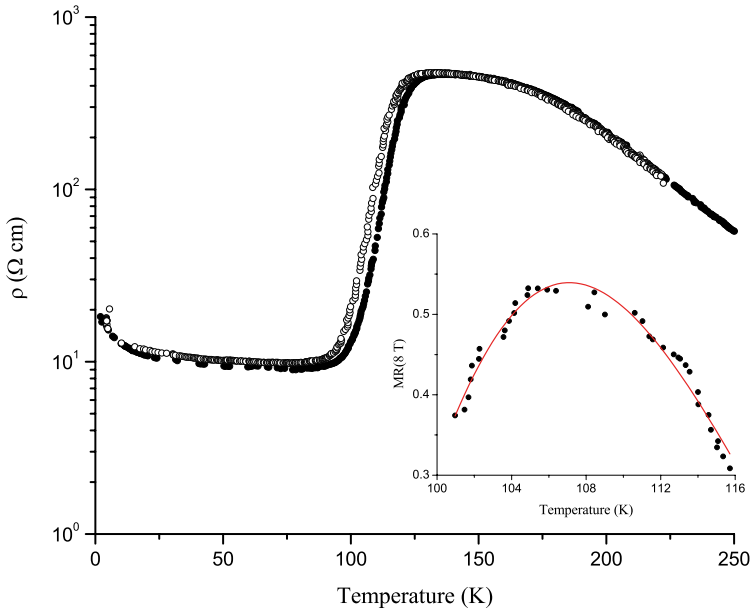

Figure 7. Temperature dependence of the electrical resistivity and magnetoresistance of $Ca_{2.5}Sr_{0.5}GaMn_2O_8$. Empty and filled circles represent resistivity measurements in fields of 0 and 80 kOe, respectively.

to magnetic order is rather broad. At high temperatures only a slow relaxation of muon polarization is observed, due to spin fluctuations in the paramagnetic state. Below 150 K this slow relaxation remains but also the initial asymmetry, $A_R(0)$, begins to fall due to the development of a static field at the muon site in a small volume fraction of the sample. The initial asymmetry only reaches its minimum near 125 K, suggesting that the entire volume of the sample is only ordered below ∼125 K. It is difficult to reconcile these observations with ordering in just 2D, and it appears that the $Ca_{2.5}Sr_{0.5}GaMn_2O_8$ undergoes phase separation into two components, one which shows 3D long-range magnetic order and another in which only 2D order is present, with the fraction of the former increasing from 0 to 1 as the sample is cooled from 150 to 125 K. The width of the transition might be attributable to the variation in local environment which is caused by the Ca/Sr disorder on the A sites within the perovskite blocks. We note that μSR is a volume technique which, unlike SQUID magnetometry, will not be sensitive to the behaviour of a 1% magnetic impurity. On cooling below 125 K the electrical conductivity of $Ca_{2.5}Sr_{0.5}GaMn_2O_8$ decreases by an order of magnitude (figure 7). However, the magnitude of the residual resistivity (∼10 Ω cm) is too great for the low-temperature phase to be described as metallic. This transition was not observed in measurements on $CaMnO_{3-\delta}$ [15, 16] and was clearest in those of our samples which contained the least impurity. We are therefore confident that it is a property of $Ca_{2.5}Sr_{0.5}GaMn_2O_8$. A magnetoresistance of ∼50% in 80 kOe is observed in the region of the transition.

The observation of a marked decrease in resistivity at a temperature close to the Néel point of $Ca_{2.5}Sr_{0.5}GaMn_2O_8$ suggests that the electronic properties of this compound may be as sensitive to composition as those of $n = 2$ $La_{2-2x}Sr_{1+2x}Mn_2O_7$ [14], and that this new family of bilayer manganates merits further investigation from the point of view not only of CMR, but also from that of fundamental science. It is interesting to note that the magnetic structure found in $Ca_{2.5}Sr_{0.5}GaMn_2O_8$ is different to all of those observed as a function of composition in the

$n = 2$ RP material, and it may be that we can learn as much from the differences between these materials as from their similarities. Most strikingly, the nearest-neighbour magnetic coupling between the two sheets of a bilayer is ferromagnetic in $Ca_{2.5}Sr_{0.5}GaMn_2O_8$, whereas it is antiferromagnetic in antiferromagnetically ordered $n = 2$ materials with a similar mean oxidation state [17]. The long Mn–O3 bond length suggests that the e_g orbital perpendicular to the sheets is the one which is occupied at those sites which are occupied by Mn^{3+}, and the ferromagnetic coupling along [010] can then be explained in terms of a σ superexchange interaction between Mn^{3+} and Mn^{4+} cations, although there is no long-range charge ordering. The presence of half-filled t_{2g} orbitals and empty e_g orbitals is consistent with the observation of antiferromagnetic coupling within the sheets. This contrasts sharply with the so-called Type A $n = 2$ materials in which the ferromagnetic coupling occurs within the individual sheets, and is strengthened by increasing the occupancy of the in-plane e_g orbital [17]. The structural differences responsible for the change in magnetic behaviour are likely to stem at least in part from the replacement of the ionic (Sr/La–O) insulating layer with a relatively covalent (Ga–O)layer.

Acknowledgments

We thank the EPSRC for financial support, and T Hansen and F Pratt for experimental assistance at ILL and ISIS, respectively.

References

[1] Urushibara A, Moritomo Y, Arima T, Asamitsu A, Kido G and Tokura Y 1995 *Phys. Rev.* B **51** 14103
[2] Moritomo Y, Asamitsu A, Kuwahara H and Tokura Y 1996 *Nature* **380** 141
[3] Ramirez A P 1997 *J. Phys.: Condens. Matter* **9** 8171
[4] Battle P D and Rosseinsky M J 1999 *Curr. Opin. Solid State Mater. Sci.* **4** 163
[5] Grenier J C, Darriet J, Pouchard M and Hagenmuller P 1976 *Mater. Res. Bull.* **11** 1219
[6] Rietveld H M 1969 *J. Appl. Crystallogr.* **2** 65
[7] Larson A C and von Dreele R B 1990 General Structure Analysis System (GSAS) *Report* LAUR 86-748 Los Alamos National Laboratories
[8] Blundell S J 1999 *Contemp. Phys.* **40** 175
[9] Wiebe C R, Greedan J E, Gardner J S, Zeng Z and Greenblatt M 2001 *Phys. Rev.* B **64** 064421-1
[10] Battle P D, Gibb T C and Lightfoot P 1990 *J. Solid State Chem.* **84** 237
[11] Battle P D, Green M A, Laskey N S, Millburn J E, Murphy L, Rosseinsky M J, Sullivan S P and Vente J F 1997 *Chem. Mater.* **9** 552
[12] Argyriou D N, Bordallo H N, Campbell B J, Cheetham A K, Cox D E, Gardner J S, Hanif K, dos Santos A and Strouse G F 2000 *Phys. Rev.* B **61** 15269
[13] Kimura T, Kumai R, Tokura Y, Li J Q and Matsui Y 1998 *Phys. Rev.* B **58** 11081
[14] Ling C D, Millburn J E, Mitchell J F, Argyriou D N, Linton J and Bordallo H N 2000 *Phys. Rev.* B **62** 15096
[15] Briático J, Alascio B, Allub R, Butera A, Caneiro A, Causa M T and Tovar M 1996 *Phys. Rev.* B **53** 14020
[16] Zeng Z, Greenblatt M and Croft M 1999 *Phys. Rev.* B **59** 8784
[17] Mitchell J F, Argyriou D N, Berger A, Grey K E, Osborn R and Welp U 2001 *J. Phys. Chem.* B **105** 10731